Atmospheric Turbulence Suppression Algorithm Based on APD Adaptive Gain Control for FSO Links of 5G Floating Base Stations

Xiaonan Yu
Lei Xiao
Shuaihe Gao
Yansong Song
Lei Zhang
Haifeng Yao
Tong Wang
Xingchi Chen
Zhiming Jin
Chang Zhou
Shoufeng Tong

Atmospheric Turbulence Suppression Algorithm Based on APD Adaptive Gain Control for FSO Links of 5G Floating Base Stations

Xiaonan Yu [1], **Lei Xiao,**[1] **Shuaihe Gao,**[2] **Yansong Song,**[1]
Lei Zhang,[1] **Haifeng Yao** [1], **Tong Wang,**[1] **Xingchi Chen,**[1]
Zhiming Jin,[1] **Chang Zhou,**[1] **and Shoufeng Tong** [1]

[1]Key laboratory of Photoelectric Measurement and Control and Optical Information Transfer Technology of Ministry of Education, Changchun University of Science and Technology, Changchun 130022, China
[2]National Time Service Center, Chinese Academy of Science, Lintong 110015, China

Abstract: The data transmission between 5G floating base stations will be an important application area of the free space optical (FSO) link, but the problem of atmospheric disturbance will directly affect the application effect. An atmospheric turbulence suppression algorithm based on avalanche photodiode adaptive gain control (APDAGC) for the laser transmission terminal was proposed to suppress atmospheric turbulence. The given design mechanism and experimental results demonstrate its function to improve the performance of FSO. When APDAGC is over 1 km FSO, the variance of intensity fluctuation is lowered from 0.046 to 0.009, with the bit error rate reduced from 4.82E-6 to 1E-12. Comparatively, as APDAGC is over 6.5 km FSO, the variance of intensity fluctuation is decreased from 1.767 to 0.376, with the bit error rate varying from 4.6E-2 to 2.4E-4. Moreover, it was used for the first FSO transmission of 5G floating base station signals on an airship platform.

Index Terms: Free space optical communication, atmospheric turbulence, avalanche photodiode, adaptive gain control, airship 5G base station.

1. Introduction

With the rapid development of the fifth generation mobile communication technology (5G), the main problem is the lack of base stations and the difficulties of site selection. In addition to the shortage of land resources in the city, the operators should also consider the cost and feasibility of station distribution in remote areas. Therefore, the establishment of airship platform-based floating 5G base station can solve the problem of remote areas and sea station distribution, and significantly improve the coverage and accessibility of 5G service [1]. However, the 5G service has a baseband transmission rate over 1 Gbps and the high-rate optical fiber communication is used in traditional base stations to complete inter-station networking and data interaction. But, for the floating base station, fiber link cannot be applied and wireless communication technology has become the only option [2]. Compared with RF wireless communication, the wireless free space optical (FSO) communication has the advantages of high communication rate, long communication distance,
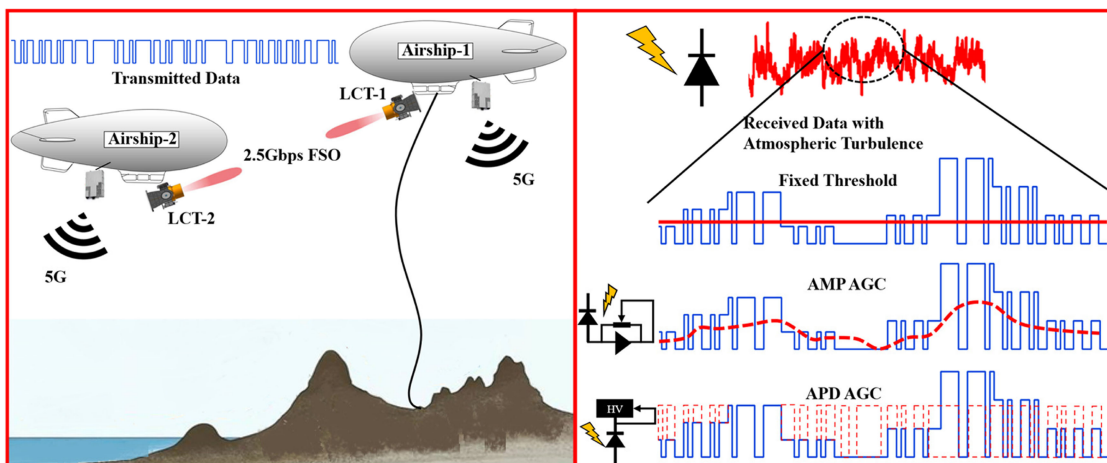
Fig. 1. Schematic diagram of the 5G floating base station and laser link (left), the mechanism and suppression measures of atmospheric turbulence flicker on the communication receiver (right).

unrestricted frequency band and low power consumption, which is the best solution to realize wireless interaction of 5G base station between floating airships [3], [4]. The above process is illustrated on the left side of the Fig. 1: there are two airships, airship1 is floating in the air over the mountains, the ground-based mooring cable uploads the 5G signal to Airship 1 and the 5G antenna on airship 1 transmits the 5G services to the users on ground and achieving the wide area coverage. And the airship 2 will float above the sea, providing 5G services to islands or vessels, while the airship 2's 5G base station signal, which is not tethered to a fiber optics cable, will rely primarily on a 2.5 Gbps rate FSO link between the laser communication terminal 1(LCT-1) and Laser communication terminal 2(LCT-2).

However, the most serious problem of wireless free space laser communication is the influence of the atmospheric channel, in which the scintillation caused by the atmosphere turbulence results in the jitter and fading of the communication data received by the receiver [5], as shown on the right side of the Fig. 1, atmospheric scintillation is superimposed on the transmitted data code, which is bound to cause a sharp rise in the bit error rate for a fixed decision threshold receiver. Many methods have been proposed to solve the scintillation problems caused by atmospheric turbulence, such as large aperture smoothing [6], [7], multi-aperture emission [8]–[10], adaptive optics [11]–[13] and channel coding [14], [15], these methods play a unique role in suppressing atmospheric turbulence, but they all bring a relatively large cost, such as the cost of volume power consumption, the loss of information transmission rate, and the increase of software and hardware complexity, this is obviously not suitable for lightweight airship applications.

From the view of communication system, the most direct way to solve the fluctuation and fading is automatic gain control (AGC). The commonly used method is the amplifier automatic gain control(AMP-AGC) shown on the right side of Fig. 1, which is to do AGC on the back-end electronic amplifier circuit. This method is similar to the adaptive threshold decision made by the comparator circuit [16], [17]. Although it can play the role of power stability and automatic decision, but the ability to suppress fading and fluctuation is still limited by the previous detector, and the dynamic range has not been improved. Therefore, the author believes that the most direct and effective way to suppress the fluctuation and fading caused by atmospheric turbulence is to carry out adaptive gain control on the front-end APD detector, namely APDAGC, the principle of this technology is that the multiplication factor of APD is controlled by the reverse bias voltage, and the general multiplication factor of APD can be adjusted from 2 times to 20 times. Therefore, in theory, the dynamic adjustment range can be expanded by 3dB-13dB, which will play an important role in suppressing atmospheric turbulence and significantly expand the dynamic range of the receiver.

This paper presents this APDAGC technology, establishes a theoretical model of APD multiplication gain control. Furthermore, the front-end photoelectric multiplication gain control mechanism to suppress light intensity fluctuations is discussed, and a precise APD current feedback and bias control circuit is designed. Then a set of PID closed-loop regulation algorithm is programmed. Experiments on suppression of turbulence in the outer field of FSO at 1 km and 6.5 km are performed after the high-bandwidth closed-loop gain control algorithm is debugged by the system, which is finally successfully used for the airship test of the 5G base station.

2. Relationship Between Atmospheric Turbulence and the BER of FSO

The design principle of this adaptive receiver is in accordance with the laser communication bit error rate model under atmospheric turbulence. This chapter primarily establishes the mathematical relationship model between atmospheric turbulence and the communication error rate.

As we know, atmospheric turbulence will give rise to fluctuations in the intensity of the laser signal. Besides, the direct response to the photodetector, namely the fading of the communication signal, will affect the judgment result, thus generating bit errors. Specifically, the intensity fluctuation resulted from atmospheric turbulence is primarily expressed quantitatively by the variance of the light intensity flicker [18], [19]:

$$\sigma_l^2 = \frac{<l^2> - <l>^2}{<l>^2} \tag{1}$$

where I represents the light intensity, and $<\cdot>$ denotes the average value. Equation 1 is the measurement statistical principle of flicker variance, and the law of flicker variance caused by atmospheric channel parameters is given below. When the Fresnel distance $(\lambda L)^{1/2} >> l_0$, the logarithmic fluctuation variance of the plane wave is [18]:

$$\sigma_l^2 = 1.23 C_n^2 k^{7/6} L^{11/6} \tag{2}$$

In the above equation, C_n^2 refers to the atmospheric refractive index structure constant; $k = 2\pi/\lambda$ is the number of the wave; L denotes the length between two terminals. Following a lognormal distribution, the normalized light intensity probability density function is expressed as follows [19]:

$$p_w(l, \sigma_l) = \frac{1}{\sqrt{2\pi\sigma_l^2}} \frac{1}{l} \exp\left[-\frac{1}{2\sigma_l^2}(\ln l)^2\right] \tag{3}$$

According to the reference [20], the near-surface atmospheric C_n^2 range 1E-13~1E-15 is considered by this paper in combination with our measurement results. In this range, the 1550 nm communication wavelength beam is set, and the link distance L is set from 0 to 7 km, with the variation of σ_l^2 being simulated as shown in Fig. 2(a) below. By combining calculation results of Equation 2, we simultaneously simulated σ_l^2 as 3, 2, 1, 0.5, and 0.1, which are actually representative values. Then, they are brought into Equation 3 to get the probability density distribution curve shown in Fig. 2(b). It should be noted that approximate calculation can merely be made under strong turbulence, since the above results have high fitting accuracy for medium and weak turbulence. The link distance dealt with in this paper is within 7 km; C_n^2 is between 1E-15 and 1E-14; σ_l^2 is within 2. In this regard, the actual situation can be better matched.

The fluctuation arising from atmospheric turbulence will exert a direct influence on the signal-to-noise ratio parameters of the detector, thereby affecting the bit error rate [21]. We define the error rate relationship of the OOK laser communication system as:

$$BER = \frac{1}{2} erfc\left[\frac{Q}{\sqrt{2}}\right] \approx \frac{\exp(-Q^2/2)}{Q\sqrt{2\pi}} \tag{4}$$

Where $Q = (A_1 - A_0)/(\sigma_1 + \sigma_0)$; A_1 and σ_1 are the signal amplitude and noise amplitude when the information bit is 1; A_0 and σ_0 denote the signal and noise amplitude as the information bit equals 0 [22]. Here we only consider the signal-to-noise ratio equation under the influence
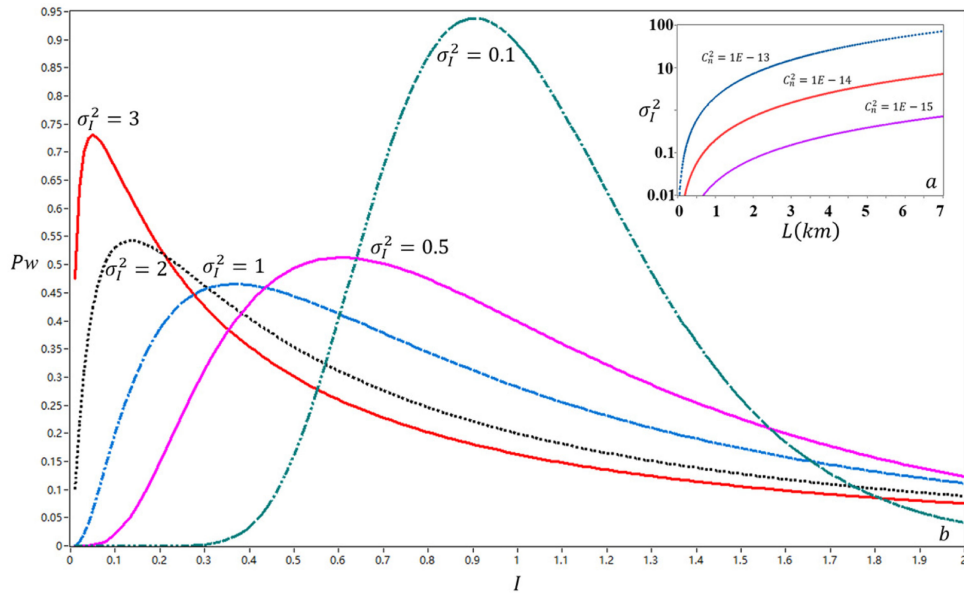
Fig. 2. (a) The relationship between L and sigma^2 (σ_I^2) under different C_n^2 conditions, (b) light intensity probability density distribution under different σ_I^2.
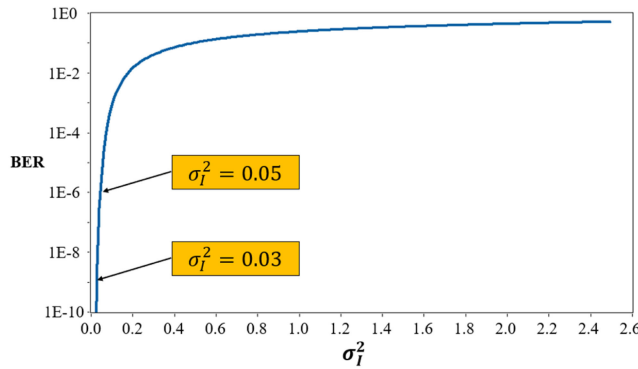

Fig. 3. Relationship between the flicker variance of light intensity and the communication bit error rate.

of atmospheric turbulence in order to establish the direct impact relationship between the flicker variance and the bit error rate, the signal-to-noise ratio expression can be acquired as follows:

$$SNR = \frac{\langle A_1^2 \rangle}{\langle \sigma_1^2 + \sigma_0^2 \rangle} = Q^2 = \frac{1}{\sigma_I^2} \tag{5}$$

Comprehensive equation (4) and (5) are conducive to the acquisition of the relationship between the flicker variance of light intensity and the communication bit error rate. Besides, the bit error rate of the flicker variance σ_I^2 from 0.02 to 2.6 is obtained through numerical simulation, as shown in Fig. 3 below:

It can be seen that it is of necessity to control the light intensity flicker variance to be within 0.05 to ensure the communication error rate below 1E-6. For the purpose of guaranteeing the communication error rate value below 1E-9, the control of the light intensity flicker variance within 0.03 is found to be essential. In summary, efficacious control concerning the variance of the light intensity flicker will effectively improve the communication error rate. In the following, the adaptive APD receiver design is employed to achieve the suppression of light intensity flicker variance.
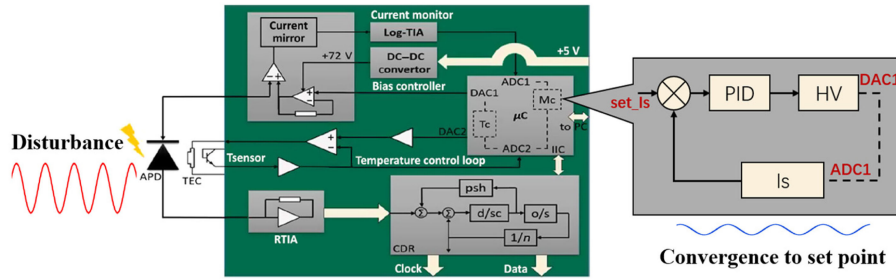
Fig. 4. APD receiver architecture diagram.

3. Scheme of Adaptive Multiplication APD Receiver

After clarifying the effect of atmospheric turbulence on the bit error rate, we consider the principle of APD gain control compensation. Concerning the algorithm of APD multiplication closed-loop adjustment, it is in line with the multiplication traits derived from the avalanche photodiode. According to the APD detection theory [23], the response equation of APD is expressed as follows:

$$i_s = \eta P_r M \qquad (6)$$

where P_r is the input optical power, i_s is the output current of the APD, η is the responsivity of the detector, and M is the multiplication factor. It is noteworthy that M has played a pivotal role in signal amplification and our gain control algorithm. The relationship between the M and the bias voltage V_R is shown as follows:

$$M = \frac{1}{1 - (V_R/V_B)^n} \qquad (7)$$

where V_B is the breakdown voltage, the Voxtel Siletz BSI RIP1-JJRC series avalanche photodiode is used in our system, according to the detector technical manual provided by reference 24, it can be seen that the break voltage V_B in this APD is 64 V, and then n is calculated as 1.62 from the gain bias curve in references [24]. When Equation 7 is introduced into Equation 6, the control effect of reverse bias voltage V_R on output current i_s can be observed, which is the principle of APD gain control.

Based on the above theory, we built the APD gain control receiver. The APD receiver is improved on the basis of the previous APD receiver [25], the previous receiver only performed gain open-loop control and overshoot current protection, and did not design a control algorithm for atmospheric turbulence, this improvement implements a closed-loop control algorithm that suppresses atmospheric turbulence. The hardware of the entire receiver is shown in Fig. 4, the cathode of the APD is the gain control terminal, including the current mirror to detect photocurrent that gives feedback to the microcontroller responsible for controlling the DAC1 to control the high-voltage power supply to adjust the APD gain. The anode of the APD is the communication output, with a transimpedance amplifier (RTIA) and clock and data recovery (CDR).

The added algorithm is a control loop, where the set current value **set_Is** is the given current expectation set by the μC (micro controller), with its value mainly resting upon the average received optical power of the laser communication link. Besides, the **Is** refers to the average photocurrent value of the APD read by ADC1 utilized as the feedback input of the control system, which then is compared with the set current **set_Is**. Then, the compensation is achieved through **PID** filtering and adjustment of the **HV** high voltage setting, with their error used as the controller input. The flow chart of the control algorithm is as follows:

As shown in the Fig. 5, under the timer interrupt of 500 us period, the average photocurrent of APD is sampled by ADC, this value is called the measured photocurrent, then the measured photocurrent is compared with the set value, resulting in a feedback error, next we should to compare the sign relationship between this error and the last integral value as the criterion for
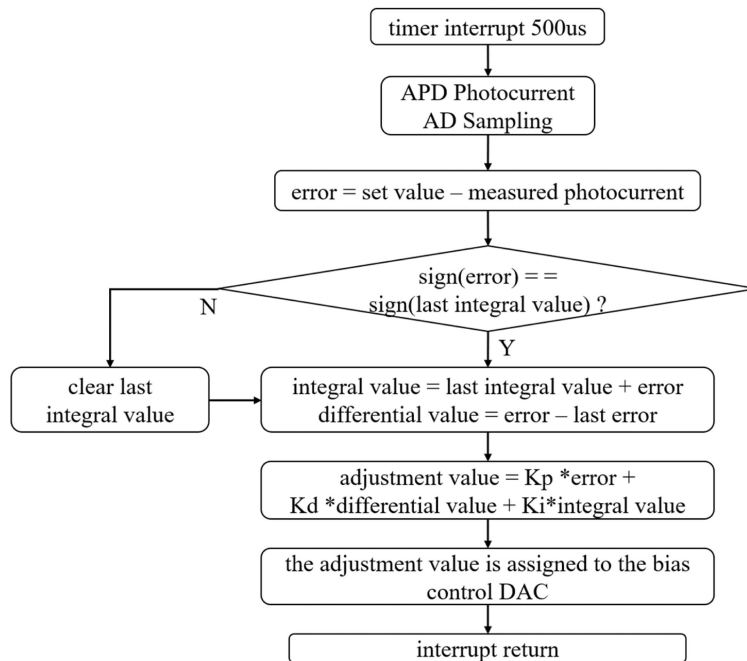
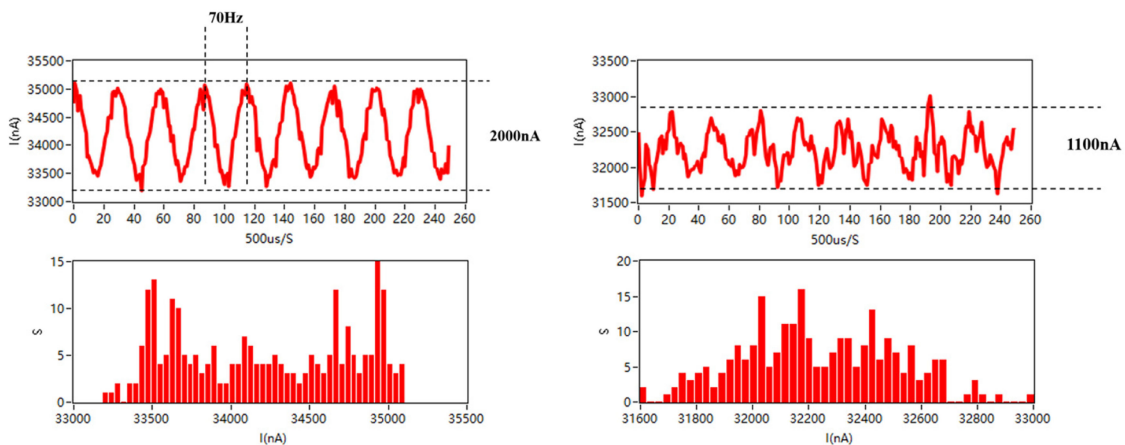Fig. 5. Flow chart of adaptive control program.

Fig. 6. Output signal of fixed gain (left) and adaptive gain (right) under the action of 70 Hz sinusoidal light intensity signal.

clearing the integral value, and then, start to generate the integral value and the differential value, the integral value is accumulated by the last integral value and the current error, and the differential value is equal to the current error minus the last error, the above is the algorithm of the PID filter and the PID parameters are debugged in the time domain, and the results are Kp = 5.23, Ki = 2.13, and Kd = 3.31, finally, the PID filtered results are sent to the DAC after amplitude matching to control the high voltage bias adjustment. After completing the design of the control system, its tracking performance has been tested, we directly measured the bandwidth of the above closed-loop tracking system by sweeping the frequency. Specifically, we use an AM modulated laser to modulate the amplitude of a sinusoidal signal, simulate the turbulent flicker, gradually increase the frequency from 1 Hz to 70 Hz, and record the amplitude-frequency characteristics and probability distribution of the output signals with and without gain control. Fig. 6 is the time-domain
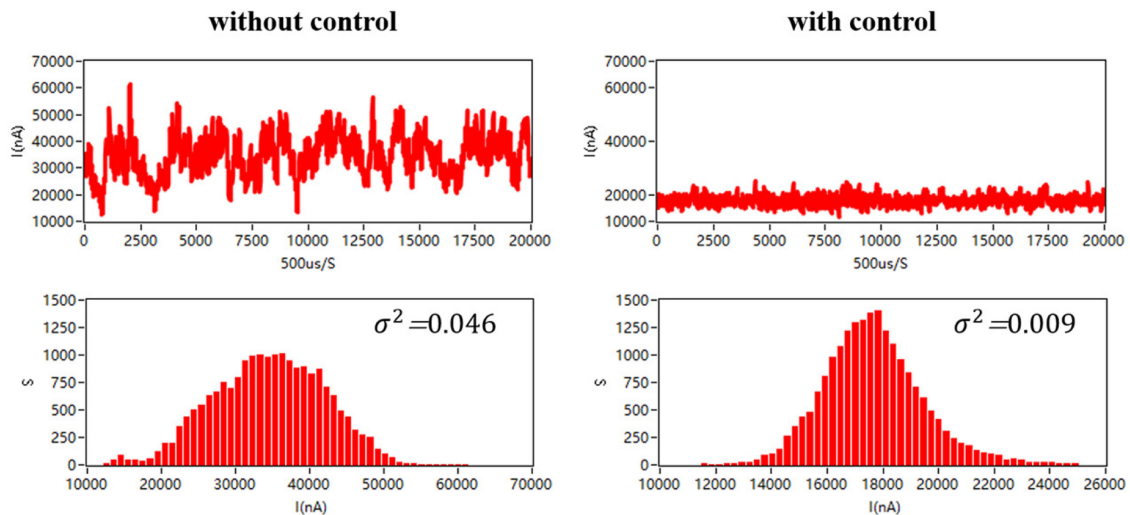
Fig. 7. Output signal results of fixed gain (left) and adaptive gain (right) under the 1km atmospheric link.

curve (up) and probability distribution (down) of the above results with (right) and without (left) gain control under the action of 70Hz sinusoidal light intensity signal.

During the test, the signal amplitude (right) after suppression increases bit by bit with the rise of frequency, indicating the gradually increasing residual error and the weakening suppression ability. When the input signal frequency reaches 70 Hz, the signal amplitude after suppression increases to the half of the output signal without control, which is the closed-loop bandwidth of the system. According to this value, the system's ability to suppress 70Hz disturbances is 50%, it means that the APD adaptive detection system can suppress the detection optical power jitter caused by atmospheric turbulent flicker in the 70Hz bandwidth to half of the unsuppressed jitter variance.

4. Experiments and Results

Based on the above theory and practice, we conducted equivalent laser communication verification experiments of both 1 km and 6.5 km. This paper aims to verify the suppression of turbulence-induced light intensity fluctuations via APD gain closed-loop control under weak and strong turbulence condition effect.

4.1 1 km FSO

First, laser communication transmission experiments between the 16th floor of the Science and Technology Building of Changchun University of Science and Technology and the 9th floor of the Teaching Building of that University are performed, with the link distance being 1 km. The experimental system consists of a laser communication transceiver with an APD receiver and a laser diode transmitter. Furthermore, a laser head unit is used for the pointing, acquisition, and tracking of the beam; a bit error rate tester is utilized to evaluate the communication performance in disparate conditions.

The conditions are defined as two sorts. One is the APD gain control not turned on, that is, the bias of the APD is a fixed value; the other is the previously designed APD adaptive gain control algorithm that is turned on. Then, the power characteristics, as well as bit error rate (Agilent N4906A) traits in these two states, are compared.
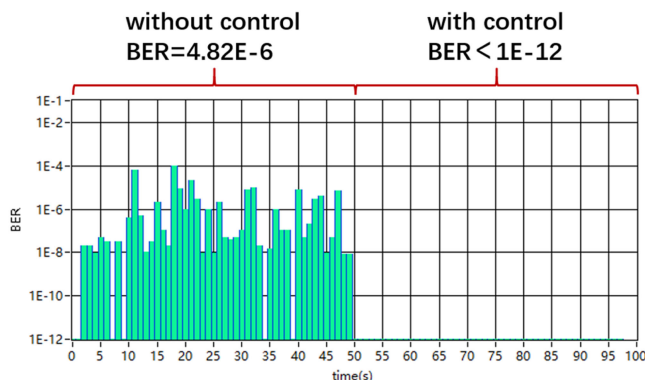
Fig. 8. Long-term bit error rate statistics for 1km link (50 s fixed gain case, 50 s adaptive gain case).

The following Fig. 7 illustrates the output optical power of APD under a 1 km atmospheric link. On the left side, the output photocurrent and its probability density distribution are reflected when APD uses a fixed gain; on the right side, they are reflected when APD uses adaptive gain control.

As shown in the left of Fig. 7, under the condition of 1 km weak turbulence, the communication optical power presents a log-normal distribution with a distribution value ranging from 10,000 nA to 70,000 nA. Besides, the flicker variance is 0.046.

When the APD gain adaptive control is added, it can be explicitly seen from the right side of Fig. 6 that the optical power becomes steady on the time domain curve. Based on the histogram of probability density distribution, the probability density is prominently concentrated, with the maximum range less than 26,000nA, showing a typical Gaussian distribution. Moreover, the flicker variance is reduced to 0.009, indicating the suppression ability of the gain control of the signal power fluctuation resulted from turbulence to a large extent.

By the error bit tester measurement, communication performance is enhanced. As shown in Fig. 8, a 2.5 Gbps laser communication link has been established to measure the communication error rate for a long time. During the entire 100 s measurement process, the first 50s is fixed by the APD Bias that presents a fixed gain state, while the last 50 s is the bit error rate under APD gain control. Then, bit error rates for the first and the last 50s data are averaged to obtain the communication performance index of 1km FSO. When the APD gain is fixed, the average bit error rate is 4.82E-6; when APD adaptive gain control is used, that rate is better than 1E-12.

4.2 6.5 km FSO

Next, the optical transceiver is placed between the 16th floor of the Science and Technology Building in Changchun University of Science and Technology and the 23rd floor of the World Trade Hotel. As the straight distance is about 6.5 km, optical transceiver parameters, as well as working and testing modes, are identical with those having straight distance of 1 km link.

On the 6.5 km link, we still detect the optical power first. In Fig. 9, there are the time domain curve and probability distribution of the optical power under fixed gain and adaptive gain, respectively.

As shown in Fig. 9, under the condition of 6.5 km medium turbulence, the communication optical power has a negative exponential distribution shape and distribution value ranges varying from 0 nA to 350,000 nA, meaning the existence of a strong fading and a fast flicker in the signal, as well as the flicker variance of 1.767. At this time, APD gain adaptive control is added, and the stability of the optical power region can be explicitly seen on the time-domain curve. Observing from the histogram of probability density distribution, we can see that the probability density is highly-centralized, with the maximum range less than 175,000nA and the flicker variance reduced to 0.376, showing similar weak turbulence. According to the logarithmic normal distribution of the light intensity flicker, the strong fading and the fast flicker of strong turbulence can be suppressed
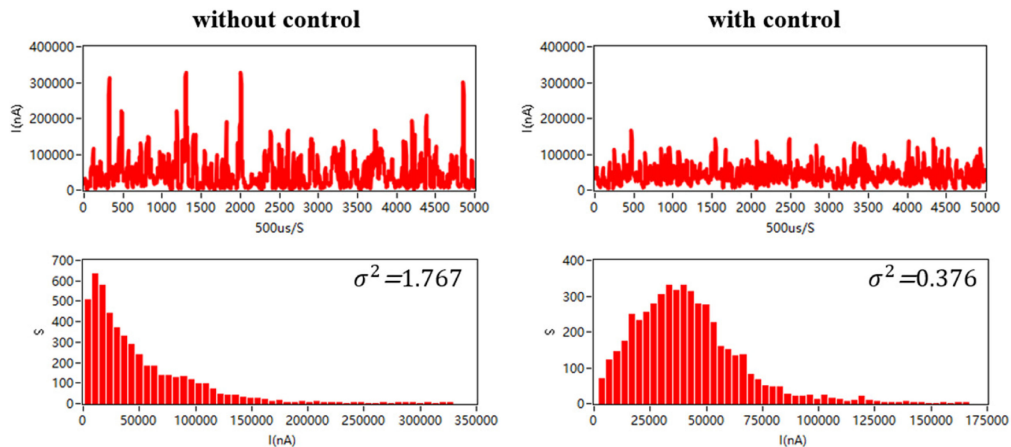
Fig. 9. Output signal results of fixed gain (left) and adaptive gain (right) under the 6.5 km atmospheric link.
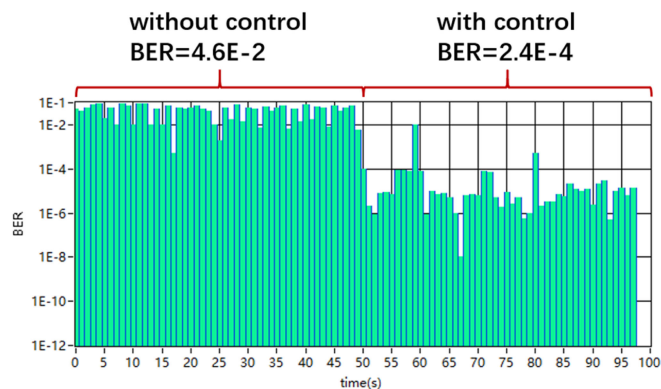

Fig. 10. Long-term bit error rate statistics for 6.5 km link (50s fixed gain case, 50s adaptive gain case).

by the gain control. Moreover, the negative exponential distribution of strong turbulence can be improved to a lognormal distribution similar to weak turbulence.

Next, as shown in Fig. 10, we performed a 100s bit error rate test experiment, in which the bit error rate is observed to deteriorate owing to the augment in flicker variance. At a fixed gain, the average bit error rate is merely 4.6E-2, but it decreases to 2.4E-4 in the case of adaptive gain. Thus, it can be seen that the gain adaptive control effectively enhances the communication quality, which is also in keeping with the previous theoretical model of the bit error rate and flicker variance.

5. Discussion and Conclusion

The above experiments show that the gain control of APD can efficaciously suppress the fluctuation of optical power generated by atmospheric turbulence jitter so as to remarkably elevate the communication error rate. For 1 km weak turbulence links, the improvement of optical power jitter variance is 0.046 / 0.009 $\approx$ 5.11 times; the corresponding power is enhanced to 7 dB; the above variance values   are taken into equations 4 and 5; the theoretical bit error rates are 1.6E-6@0.046 and 2.8E-26@0.009, which are matched with the actual observed average bit error rate of 4.82E-6@0.046 and <1E-12@0.009, respectively; the actual bit error rate is improved by more than 6 orders of magnitude. In terms of the 6.5 km strong turbulence state, the improvement of the variance concerning the optical power jitter is 1.767 / 0.376 $\approx$ 4.67 times, and the corresponding power is enhanced by 6.7 dB. Similarly, the bit error rate obtained after introducing Equations 4 and

Fig. 11. Airship to ground 5G base station laser transmission.

5 is 4.0E- 1@1.767 and 6.5E-2@0.376, respectively. Under the circumstance of strong turbulence, the actual observed bit error rate is better than the theoretical calculation result, possibly owing to the fact that the strong turbulence probability density distribution tends to be negative exponential distribution. However, the overall improvement has reached 2 orders of magnitude from 4.6E-2 @1.767 to 2.4E-4@0.376.

The above technology and results have been applied in the design of 5G laser terminal receiver, and the actual field application has been carried out. We conducted a verification test of the air link between the airship 5G node and the 5G node on the ground of Jingmen, Hubei, and broadcast the 5G signals, the main significance of which lies in the realization of 5G base station coverage in ocean and remote areas considering that 5G base station is moved to the air. Transmitted step by step through the FSO link instead of optical fiber, 5G signals between base stations finally reach the ground and connect to the 5G network. The test is shown in Fig. 11 below. With a distance of 1 km, the airship and the ground station are both equipped with the 5G broadcast base station and an FSO terminal. After the FSO link is established, the 5G data on the airship is transmitted to the ground station by 2.5 Gbps laser signal, and the ground station broadcasts to the user through the 5G base station. The 5G downlink data rate measured by the user is 854 Mbps, and the uplink data rate is 149 Mbps.

The first laser retransmission 5G experiment proves the feasibility for the air platform base station to forward 5G signals and the effectiveness of the APD adaptive control algorithm for atmospheric laser communication. According to the plan, the current experiment is only a two-way laser link between the airship and the ground, but in the future, it will be gradually upgraded to the link between the airships described in the previous blueprint.

The above theories and experiments show that APDAGC is an effective method to suppress the influence of atmospheric turbulence on free space laser communication, which will provide technical assistance for the future FSO to gradually improve and industrialize, and also opens a window for the commercialization of FSO, the commercialization of FSO links will lay the foundation for the 5G air platform base station networking, and realize the global laser space network 5G broadcast air base stations.

References

[1] Z. Gu, J. Zhang, Y. Ji, L. Bai and X. Sun, "Network topology reconfiguration for FSO-based Fronthaul/Backhaul in 5G+ wireless networks," *IEEE Access*, vol. 6, no. 99, 2018, Art. no. 18495784.

[2] M. Alzenad, M. Z. Shakir, H. Yanikomeroglu, and M. S. Alouini, "FSO-based vertical backhaul/fronthaul frameword for 5G+ wireless networks," *IEEE Commun. Mag.*, vol. 56, no. 1, pp. 218–224, Jan. 2018.

[3] J. C. Juarez, R. A. Venkat, R. Luna, D. A. Kitchin, M. E. Jansen, and D. W. Young, "Free space optical communication," *Optoelecfronic Technol.*, vol. 32, no. 1, 26–30, 2017.

[4] H. Kaushal, V. K. Jain, and S. Kar, "Free space optical communication," *De Gruyter*, 2017.

[5] L. Yang, B. Zhu, J. Cheng, and J. F. Holzman, "Free-space optical communications using on-off keying and source information transformation," *J. Lightw. Technol.*, vol. 34, no. 11, pp. 2601–2609, Jun. 1, 2016.

[6] H. Yuksel and C. C. Davis, "Aperture averaging for studies of atmospheric turbulence and optimization of free space optical communication links," in *Proc. SPIE – Int. Soc. Opt. Eng.*, 2005, 63041E1–63041E11.

[7] H. Yuksel, S. Milner, and C. C. Davis, "Aperture averaging for optimizing receiver design and system performance on free-space optical communication links," *J. Opt. Netwo.*, vol. 4, no. 8, pp. 462–475, 2005.

[8] E. J. Lee and V. W. S. Chan, "Diversity coherent and incoherent receivers for free-space optical communication in the presence and absence of interference," *J. Opt. Commun. Netw.*, vol. 1, no. 5, pp. 463–483 (2009).

[9] Y. Cai, Y. Chen, H. T. Eyyuboglu, and H. T. Lu, "Propagation of laser array beams in a turbulent atmosphere," *Appl. Phys. B: Laser Opt.*, vol. 88, no. 3, pp. 467–475, 2007.

[10] F. Pan and S. Y. Yu, "Scintillation characterization of multiple transmitters for ground-to-satellite laser communication," *Photon. Asia; Sensors Imag.*, vol. 5640, 2004.

[11] W. H. Jiang, "Adaptive optical technology," *Chin. J. Nature*, vol. 28, no. 1, pp. 7–13, 2005.

[12] M. Li and M. Cvijetic, "Coherent free space optics communications over the maritime atmosphere with use of adaptive optics for beam wavefront correction," *Appl. Opt.*, vol. 54, no. 6, pp. 1453–1462, 2015.

[13] G. Z. Antonio, C. V. Carmen, and C. V. Beatriz, "Rate-adaptive FSO links over atmospheric turbulence channels by jointly using repetition coding and silence periods," *Opt. Express*, vol. 18, no. 24, pp. 25422–254340, 2010.

[14] X. L. Sun, D. Zou, Z. Qu, and I. B. Djordjevic, "Run-time reconfigurable adaptive LDPC coding for optical channels," *Opt. Express*, vol. 26, no. 22, 29319–29329, 2018.

[15] Y. Zhang, P. Wang, T. Liu, L. X. Guo, T. Yu, and W. Wang, "Performance analysis of a LDPC coded OAM-based UCA FSO system exploring linear equalization with channel estimation over atmospheric turbulence," *Opt. Express*, vol. 26, no. 17, pp. 22182–22196, 2018.

[16] S. Ding, J. Zhang, and A. Dang, "Adaptive threshold decision for on-off keying transmission systems in atmospheric turbulence," *Opt. Express*, vol. 25, no. 20, pp. 24425–24436, 2017.

[17] S. M. Kim, "An algorithm for bit error rate monitoring and adaptive decision threshold optimization based on pseudo-error counting scheme," *J. Opt. Soc. Korea*, vol. 14, 1, pp. 22–27, 2010.

[18] J. Jiang, J. Ma, L. Tan, S. Yu, and W. Du, "Measurement of optical intensity fluctuation over an 11.8 km turbulent path," *Opt. Express*, vol. 16, no. 10, pp. 6963–6973, 2008.

[19] N. T. Dang and A. T. Pham, "Performance improvement of FSO/CDMA systems over dispersive turbulence channel using multi-wavelength PPM signaling," *Opt. Express*, vol. 20, no. 24, pp. 26786–26797, 2012.

[20] J. Qi, L. Song, X. Ni, Y. Liu, and Z. Liu, "Measurement of optical intensity fluctuation over a real atmospheric turbulent path," in *Proc. IEEE Int. Conf. Optoelectronics Microelectronics*, 2015, pp. 16–18.

[21] Y. Li, M. Li, Y. Poo, J. Ding, M. Tang, and Y. Lu, "Performance analysis of OOK, BPSK, QPSK modulation schemes in uplink of ground-to-satellite laser communication system under atmospheric fluctuation," *Opt. Commun.*, vol. 317, pp. 57–61, 2014.

[22] H. Li and X. Sang, "SNR and transmission error rate for remote laser communication system in real atmosphere channel," *Sensors Actuators A Physical*, vol. 258, pp. 156–163, 2017.

[23] A. Yariv and P. Yeh, *Photonics: Optical Electronics in Modern Communications*, Oxford, U.K.: Oxford Univ. Press, Inc, 2006.

[24] Voxtel, Inc, "Siletz BSI RIP1-JJRC 75um, 2.2 GHz photoreceiver user guide," 2012.

[25] X. N. Yu, S. F. Tong, Y. Dong, Y. S. Song, S. C. Hao, and J. Lu, "Design and performance testing of an avalanche photodiode receiver with multiplication gain control algorithm for intersatellite laser communication," *Opt. Eng.*, vol. 55, no. 6, 2016, Art. no. 067109.